Hybrid Plasmonics Slot THz Waveguide for Subwavelength Field Confinement and Crosstalk between Two Waveguides

Xiao, Jing; Wei, Qi-Qin; Yang, Duo Guo; Zhang, Ping; He, Ning; Zhang, Guo Qi; Chen, Xian Ping

DOI
10.1109/JSTQE.2017.2649939

Publication date
2017

Document Version
Final published version

Published in
IEEE Journal of Selected Topics in Quantum Electronics

Hybrid Plasmonics Slot THz Waveguide for Subwavelength Field Confinement and Crosstalk Between Two Waveguides

Jing Xiao, Qi-Qin Wei, Duo-Guo Yang, Ping Zhang, Ning He, Guo-Qi Zhang, *Fellow, IEEE*, and Xian-Ping Chen

***Abstract*—The slot waveguide has attracted considerable attention because of its ability to confine and guide electromagnetic energy at the subwavelength scale beyond the diffraction limit. We propose a novel terahertz slot waveguide structure to achieve a better tradeoff between propagation length and field confinement capacity, the novel waveguide consisting of a two slot structure. The performances of terahertz waveguides were investigated using the finite-element method. The results demonstrated that the hybrid slot waveguide (HSW) provides significantly enhanced field confinement in low index slot regions: more than five times that of traditional low index slot waveguides (LISWs). An optimized HSW structure was achieved by tuning the tradeoff between mode confinement and propagation length. We also showed that its integration in conventional planar waveguide circuits was greatly improved compared with the LISWs, by comparing their crosstalk. The proposed new HSW structure has great potential to enable THz production of compact integration and could lead to true semiconductor-basedTHz applications with high performance.**

***Index Terms*—Terahertz radiation, slot THz waveguide, enhanced field, propagation length, crosstalk.**

I. Introduction

TERAHERTZ waveguides have attracted significant attention in recent years due to their potential applications in a variety of areas, such as pharmaceutical quality control [1], [2], medical diagnostics [3], [4], imaging [5]–[7] and sensory applications [8]–[10]. Terahertz radiation (THz), which is situated between infrared and microwave radiation on the electromagnetic spectrum, typically refers to frequencies from 100 GHz to 30 THz [3], [4], [11]. With the commercialization of terahertz wave sources and detectors as an essential part of terahertz science and technology, THz waveguides have attracted considerable attention and their investigation has rapidly progressed in recent years [12]. During the past few decades, many researchers attempted to development the dual goal of low loss and smaller-sized THz waveguides. Examples include dielectric waveguides [13]–[17], metallic waveguides [18]–[21] and plasmonic waveguides [22], [23]; these structures have all been theoretically proposed or experimentally demonstrated. Among the wide variety of THz waveguide structures being investigated, plasmonic structures can achieve a better tradeoff between propagation length and confinement capacity. In addition, plasmonic waveguides can break through the diffraction limitation and achieve a smaller physical size. However, surface plasmon polaritons (SPPs) only give subwavelength field localization for frequencies close to the intrinsic plasma frequency of the conductor [19]. In the THz regime, metals are nearly a prefect conductor and negligible penetration of electromagnetic fields leads to highly delocalized surface plasmon polaritons [19], [24]. Besides this, the problem of loss in THz waveguide has become the largest obstacle for migration from theoretical predictions to practical implementations.

In order to provide a solution for the above problem, we propose a novel layer-by-layer metal–semiconductor–slot–semiconductor–metal structure that we call a hybrid slot waveguide (HSW), because the silicon-slot-silicon was superimposed over a metal-slot-metal. The characteristics of its integration properties were investigated using the finite-element method. Firstly, we studied the electric field distribution of fundamental slot modes and the dual-plasmonics slots effect; the low-index polyethylene (LDPE) layer showed a good subwavelength in THz field confinement. To find out the appropriate layer height for the HSW, the effect of the height on field confinement and field distribution was analysed. After that, the field confinement of our proposed HSW structure was further investigated by comparing it with the low-index slot waveguides (LISWs) which have a low-index slot layer embedded in a homogeneous high-index material. Finally, the properties of on-chip integrations(crosstalk) with the HSW structure were also studied and compared with the LISW structure. The proposed HSW structure was easy to fabricate using layer-by-layer deposition and formation by chemical etching. It exhibits improved crosstalk between two same waveguides in THz circuits.

Manuscript received September 30, 2016; revised November 27, 2016; accepted January 4, 2017. Date of publication January 9, 2017; date of current version March 2, 2017. The work was supported in part by the Natural Science Foundation of China under Grant 51303033, Grant 51366003, and Grant 61461014, and in part by the Innovation Project of Guangxi Graduate Education under Grant YCBZ2015037.

J. Xiao, Q.-Q Wei, D.-G. Yang, P. Zhang, and N. He are with the School of Electronic Mechanical and Electrical Engineering, Guilin University of Electronic Technology, Guilin 541004, China (e-mail: xiaojing@guet.edu.cn; 570149087@qq.com; daoguo_yang@vip.163.com; zp3631@gmail.com; eicnhe@guet.edu.cn).

G.-Q. Zhang is with the Delft Institute of Mircosystems and Nanoelectronics, Delft University of Technology, Delft 2628 CD, The Netherland (e-mail: G.Q.Zhang@tudelft.nl).

X.-P. Chen is with the College of Opto-Electronic Engineering, Chongqing University, Chongqing 400044, China (e-mail: xianpingchen@cqu.edu.cn).

Color versions of one or more of the figures in this paper are available online at http://ieeexplore.ieee.org.

Digital Object Identifier 10.1109/JSTQE.2017.2649939

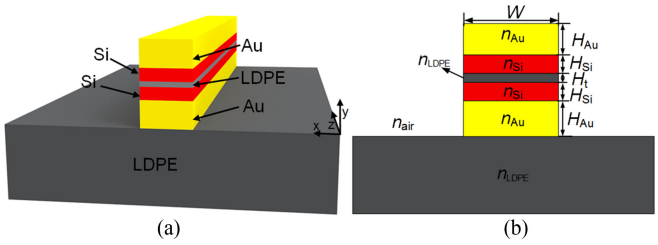

Fig. 1. (a) 3D and (b) 2D cross-section geometries of the proposed HSW.

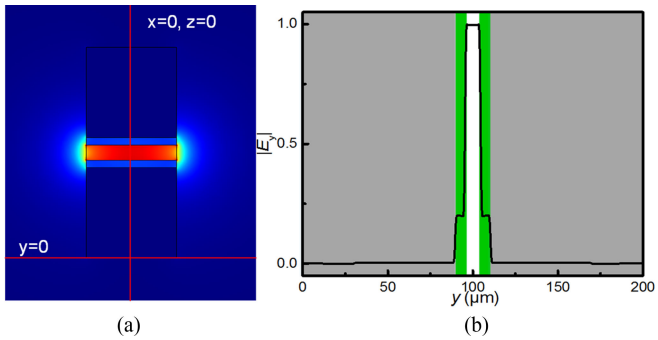

Fig. 2. (a) A 2D electric field distribution of the fundamental modes of HSW; (b) The corresponding field profiles in the y-axis (E_y) for HSW.

II. Proposed Waveguide Structure and Simulations

Three-dimensional (3D) geometries and two-dimensional (2D) cross sections of the proposed HSW are illustrated in Fig. 1(a) and (b), respectively. Instead of the silicon inserted by low-index layer structures in the original design, the proposed HSW structure is comprised of a metal ridge, semiconductor ridge, low-index slot ridge, semiconductor ridge and metal ridge on the horizontal substrate. The metal, semiconductor, and low-index insulating layers were Au, Si, and low-density polyethylene (LDPE), respectively. We defined the width of the HSW as W and the height of Au layers, Si layers and LDPE layers as H_{Au}, H_{Si}, and H_t, respectively. In our simulations, we set the wavelength λ as 0.3 mm. The refractive indices in $\lambda = 0.3$ mm of Si, Au, and air were $n_{\mathrm{Si}} = 3.415 + 0.0000198\mathrm{i}$, $n_{\mathrm{Au}} = 554 + 646\mathrm{i}$ and $n_{\mathrm{air}} = 1$, respectively. The refractive index of the dielectric layer, n_{LDPE}, was $1.51 + 0.000478\mathrm{i}$ [25]. All the simulations were conducted using the finite element method (FEM) in COMSOL. The calculation region was given with scattering boundary conditions. A convergence analysis was conducted to ensure that the meshing, boundary conditions and associated calculation parameters were sound.

III. Results and Discussion

At the beginning of this study, we investigated the electric field distributions of the fundamental slot mode. The dimensions of the HSW were $W = 60\,\mu$m, $H_{\mathrm{Au}} = 60\,\mu$m, $H_{\mathrm{Si}} = 5\,\mu$m, and $H_t = 10\,\mu$m. The results of the electric field distributions are shown in Fig. 2(a). It is clearly seen that the electric field is enhanced in regions where the layer is between the two Si layers. Fig. 2(b) more clearly shows the difference in intensity of the y component of the electric field (E_y) of the slot.

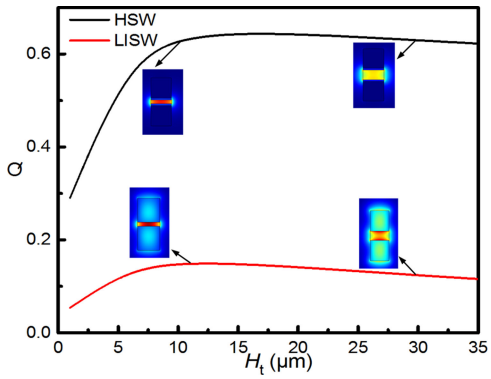

Fig. 3. Confinement factor (Q) of HSW (or LISW) as a function of the height of low-index layer (H_t).

Ultra-strong field enhancement in the vertical direction was observed in the low-index LDPE layers, which is beneficial for the low-index slot, with $H_t = 10\,\mu$m, embedded between the Si layers. Furthermore, an intensity enhancement of the electric field was also presented between the two plasmonics structures made of Si layers and Au layers, because the field enhancement at the boundary in the low-index region came from a hybrid effect of Si and Au. This structure is capable of realizing a high confinement factor for a quasi-TM mode. The coupling issues in such waveguide is a challenge, but it can be solved according to some reference [26], [27].

To further characterize the working performances, we compared the field confinement capability of the HSW structure with LISW at different widths. Here, we set $H_t = 60\,\mu$m, $H_{\mathrm{Si}} = 5\,\mu$m, $H_{\mathrm{Au}} = 10\,\mu$m. In order to further investigate the HSW's behavior in field confinement, the confinement factor was defined as $Q = P_1/P_2$, where P_1 is the power density inside the low-index slot regions and P_2 is the power density which is distributed throughout the structures. The confinement factor (Q) versus the height (H_t) of the low-index layers for both HSW and LISW was plotted and shown in Fig. 3. It is evident that the values of Q for HSW and LISW exhibited similar changes depending on H_t. The values of Q for HSW increased with the increase of H_t from 1 to 10 μm. At $H_t = 15\,\mu$m, the value reached a maximum of 64.47%; after that, it remained at about the same value. For LISW, the variation of Q had a similar trend to HSW within the range of H_t from 1 to 11 μm. At $H_t = 11\ \mu$m, the value of Q for LISW reached a maximum of 15.09%; after that, it decreased with increasing H_t. It is important to note that the value of Q for HSW was much higher than that of LISW at the range of H_t from 1 to 35 μm. For instance, the fundament modal profiles for both HSW and LISW at $H_t = 11\ \mu$m and 30 μm have been shown in the insets of Fig. 3 and it is notable that at $H_t = 30\,\mu$m, HSW has kept a good field confinement capability, while LISW has less energy in the low index layer. These results demonstrate that the field confinement capability of the HSW is better than that of the traditional LISW. Two effects on the field confinement property are associated with the proposed HSW structure. One is that more energy can be confined in the slot between the plasmonics structure than the slot in the silicon. The other is that some

energy can overflow from the middle layer to the Si layer in LISW structure due to the slot area comprised of silicon. A substantial amount of THz electromagnetic energy can be held in the slot region; a structure with this property has promising use in various practical applications such as high-speed communication, molecular spectroscopy, security imaging and medical diagnosis.

As found above, the HSW structure can provide enhanced field confinement. However, field enhancement means that the propagation length will decline [28], [29]. Therefore, the design was optimized to provide a better tradeoff between field confinement and propagation loss [29]. THz electromagnetic energy can be transmitted in the silicon, so the height of the silicon area is an important factor in the properties of the proposed waveguide. The parameter of silicon's height (H_{si}) can control the field confinement properties of the HSW, which was set to 5 μm, 10 μm, 15 μm, and 20 μm. The properties of the HSW were affected by the slot ridge between two silicon layers. The confinement ability can be expressed as the normalized effective mode area (A_{eff}/A_0), where A_0 is the diffraction-limited mode area in free space, defined as $\lambda^2/4$. Therefore the target parameters of optimization were A_{eff}/A_0 and the propagation length (L). The propagation length of structure was defined as

$$L = \lambda / \left(4\pi\, Im\left(n_{\mathrm{eff}}\right)\right) \tag{1}$$

where n_{eff} is the complex modal effective index, and the effective mode area A_{eff} was calculated by

$$A_{\mathrm{eff}} = [\iint W(\boldsymbol{r})dA]/\{\max(W(\boldsymbol{r}) \tag{2}$$

where the electromagnetic energy density $W(r)$ was defined as [14]

$$W\left(\boldsymbol{r}\right) = \frac{1}{2}\mathrm{Re}\left\{\frac{d\left[\omega\varepsilon\left(\boldsymbol{r}\right)\right]}{d\omega}\right\}\left|E\left(\boldsymbol{r}\right)\right|^2 + \frac{1}{2}\mu_0\left|H\left(\boldsymbol{r}\right)\right|^2 \tag{3}$$

where $E(r)$ and $H(r)$ are the electric and magnetic fields, $\varepsilon(r)$ is the electric permittivity, and μ_0 is the vacuum permeability or magnetic constant. To compare the performance of different configurations, a figure of merit (FOM) was introduced, which was defined as: $\mathrm{FOM} = L/[2(A_{\mathrm{eff}}/\pi)^{1/2}]$. The effect of H_t and H_{Si} on $Im(n_{\mathrm{eff}})$, L, A_{eff}/A_0 and FOM is shown in Fig. 4(a)–(d), respectively. From Fig. 4(a), it can be seen that when $H_t < 20\,\mu$m, $Im(n_{\mathrm{eff}})$ decreased as H_{Si} increases, implying that the transmission loss decreased with the increase of H_{Si}. On the contrary, when $H_t < 20\,\mu$m, the propagation length (L) always increased with the increase of H_{Si} [see Fig. 4(b)]. It is noted that the value of $Im(n_{\mathrm{eff}})$ and L tend to be stable, showing that the loss of propagation was independent of H_t.

We also observed that A_{eff}/A_0 can be enhanced by increasing H_{Si}, H_t, or both, as shown in Fig. 4(c), which means the field confinement capability has a negative dependence on H_{Si}, H_t, or both. This is because the ability of metal to confine electromagnetic energy is greater than that of non-metals. Even when $H_{\mathrm{Si}} = 20\,\mu$m, the electromagnetic energy was confined to the subwavelength area.

Using the L/H_t data in Fig. 4(b) together with the $(A_{\mathrm{eff}}/A_0)/H_t$ data in Fig. 4(c), it was possible to derive

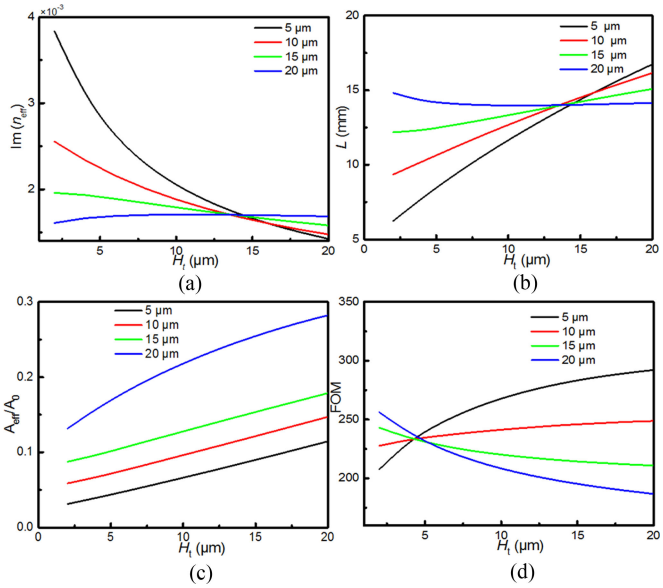

Fig. 4. Dependence of (a) $Im(n_{\mathrm{eff}})$, (b) L, (c) the normalized effective mode area (A_{eff}/A_0), (d) the FOM of the fundamental mode of the HSW on the height of the center slot H_t.

the relationship between FOM and H_t for each H_{Si}, as shown in Fig. 4(d). FOM increased with increasing H_t, when $H_{\mathrm{Si}} = 5\,\mu$m and $H_{\mathrm{Si}} = 10\,\mu$m. However, FOM decreased with $H_{\mathrm{Si}} = 15\,\mu$m and $H_{\mathrm{Si}} = 20\,\mu$m. Based on the data of Fig. 4(d), the optimal HSW configuration with the best tradeoff between field confinement ($A_{\mathrm{eff}}/\mathrm{A}_0 = 0.169$) and propagation length ($L = 14.23$ mm) was achieved at $H_{\mathrm{Au}} = 60\,\mu$m, $H_{\mathrm{Si}} = 20\,\mu$m, and $H_t = 5\,\mu$m. In this case, n_{eff} was 1.758.

The integration properties of slot waveguide structures can be characterized by crosstalk. In the following text, the crosstalk of the optimized HSW structure is evaluated. Because of the existence of metal on the top of the structure, the crosstalk in the vertical direction is relatively small. Hence, only horizontal crosstalk was investigated to predict the integration properties. The crosstalk can be featured by the coupling length (L_c) and the maximum transfer power ($P_{\max}$). The coupling length L_c can be calculated by [30]–[32]

$$L_c = \pi / \left|k_s - k_a\right| \tag{4}$$

where k_s and k_a are the wavenumbers of the symmetric and anti-symmetric modes of two coupled waveguides, respectively. The maximum transfer power is a function of L_c [32]

$$P_{\max} = \frac{\exp\left(-2 * x * arctan\left(x^{-1}\right)\right)}{1 + x^2} \tag{5}$$

where

$$x = 2L_c / \left(\pi L_P\right), \tag{6}$$

if L_p is the mean attenuation length of the symmetric and anti-symmetric modes of two couple waveguides.

In order to calculate the coupling length and maximum transfer power, the anti-symmetric and symmetric crosstalk systems (which consist of two identical HSW waveguides) were built as schematically shown in Fig. 5(a) and (b), respectively. For

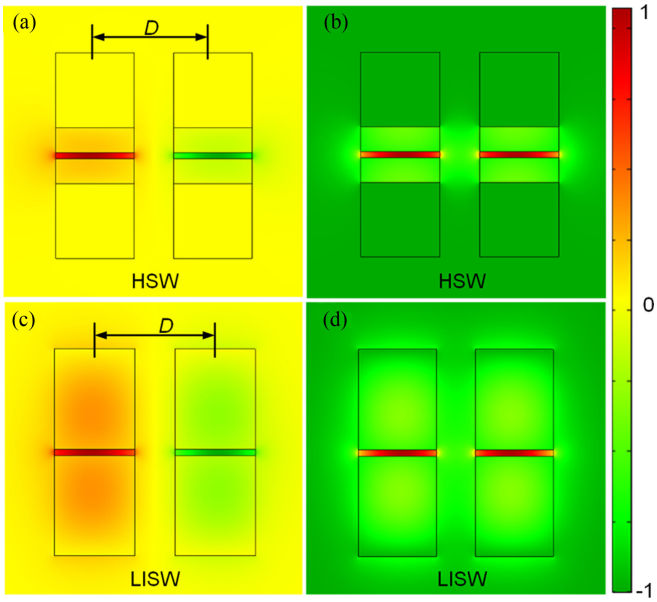

Fig. 5. The Ey field distributions of (a) the anti-symmetric two HSWs; (b) the symmetric two HSWs; (c) the anti-symmetric two LISWs and (d) symmetric two LISWs with a distance of D $= 30\,\mu$m.

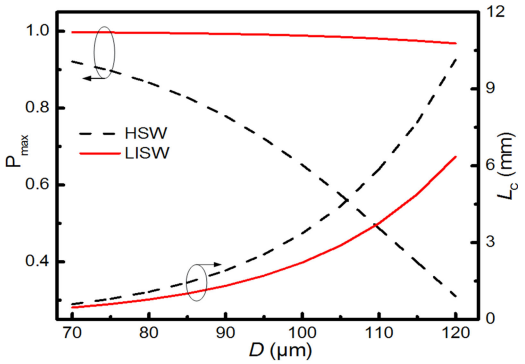

Fig. 6. The coupling length and the maximum transfer power on the center-to-center distance, *D*, between two coupling HSWs and LISWs.

comparison, the anti-symmetric and symmetric crosstalk systems (which consist of two identical LISW waveguides) were also built as schematically shown in Fig. 5(c) and (d), respectively.

The center-to-center separation distance between two waveguides in crosstalk systems is defined as *D*. The coupling length L_c and the maximum transfer power was plotted as a function of the distance *D* in Fig. 6 for both HSW and LISW; the coupling length (L_c) increased monotonically with increasing separation distance. It is of interest to note that with the same *D*, the coupling length of HSW was much longer than that of LISW. Besides this, for HSW, the maximum transfer dramatically decreased with increasing distance. However, for LISW, not only did the maximum transfer power have a small decrease with increase of *D*, but it was also much larger than HSW under same conditions. These results indicate that our proposed HSW structure has much lower crosstalk compared with the LISW structure. The lower crosstalk can be attributed to the enhanced confinement capability in the HSW structure which can help to reduce the mode overlap between two waveguides. Our results revealed that the proposed HSW structure can provide higher density integration in integrated photonic circuits.

IV. Conclusion

To develop THz integration technology, a novel terahertz slot waveguide structure has been proposed and its field mode characteristics and horizontal crosstalk have been investigated using the finite element method. Comprehensive theoretical computations showed that the proposed slot waveguide structure is capable of enhancing electromagnetic confinement at THz wavelengths ($\lambda = 0.3$ mm) as compared to LISWs, because the plasmonics slot function is guarded by semiconductors and metal. Optimization of the HSW structure achieves 2D tight mode confinement with relatively low propagation loss (the propagation length can reach 14.23 mm). Moreover, the optimized HSW structure exhibits better planar integration(crosstalk) properties than that of LISWs, providing the capability for high density integration in Si-based electronic circuits and planar THz wave circuits. Our proposed HSW structure can be made using a standard Si fabrication process and has the potential to enable the production of compact THz components.

References

[1] C. J. Strachan *et al.*, "Using terahertz pulsed spectroscopy to quantify pharmaceutical polymorphism and crystallinity," *J. Pharmaceutical Sci.*, vol. 94, no. 4, pp. 837–846, 2005.
[2] S. Atakaramians, S. Afshar, T. M. Monro, and D. Abbott, "Terahertz dielectric waveguides," *Adv. Opt. Photon.*, vol. 5, no. 2, pp. 169–215, 2013.
[3] B. Ferguson and X.-C. Zhang, "Materials for terahertz science and technology," *Nature Mater.*, vol. 1, no. 1, pp. 26–33, 2002.
[4] M. Tonouchi, "Cutting-edge terahertz technology," *Nature Photon.*, vol. 1, no. 2, pp. 97–105, 2007.
[5] C. R. Williams *et al.*, "Highly confined guiding of terahertz surface plasmon polaritons on structured metal surfaces," *Nature Photon.*, vol. 2, no. 3, pp. 175–179, 2008.
[6] Z. Ghattan, T. Hasek, R. Wilk, M. Shahabadi, and M. Koch, "Sub-terahertz on–off switch based on a two-dimensional photonic crystal infiltrated by liquid crystals," *Opt. Commun.*, vol. 281, no. 18, pp. 4623–4625, 2008.
[7] H. T. Chen, R. Kersting, and G. C. Cho, "Terahertz imaging with nanometer resolution," *Appl. Phys. Lett.*, vol. 83, no. 15, pp. 3009–3011, 2003.
[8] K. Yamamoto *et al.*, "Noninvasive inspection of C-4 Explosive in mails by terahertz time-domain spectroscopy," *Jpn. J. Appl. Phys.*, vol. 43, no. 3, pp. L414–L417, 2004.
[9] M. Nagel, P. Haring Bolivar, M. Brucherseifer, and H. Kurz, "Integrated THz technology for label-free genetic diagnostics," *Appl. Phys. Lett.*, vol. 80, no. 1, pp. 154–156, 2002.
[10] M. Nagel *et al.*, "THz technology for label-free genetic diagnostics," in *Proc. Annu. Meet. IEEE Lasers Electro-Opt. Soc.*, 2002, vol. 1, pp. 345–346.
[11] S. P. Mickan and X. C. Zhang, "T-ray sensing and imaging," *Proc. IEEE*, vol. 95, no. 8, pp. 1528–1558, Aug. 2007.
[12] J. S. Li, H. Liu, and L. Zhang, "Compact and tunable-multichannel terahertz wave filter," *IEEE Trans. THz. Sci. Technol.*, vol. 5, no. 4, pp. 551–555, Jul. 2015.
[13] O. Mitrofanov, R. James, F. A. Fernández, T. K. Mavrogordatos, and J. A. Harrington, "Reducing transmission losses in hollow THz waveguides," *IEEE Trans. THz. Sci. Technol.*, vol. 1, no. 1, pp. 124–132, Sep. 2011.
[14] B. Bowden, J. A. Harrington, and O. Mitrofanov, "Low-loss modes in hollow metallic terahertz waveguides with dielectric coatings," *Appl. Phys. Lett.*, vol. 93, no. 18, 2008, Art. no. 181104.
[15] B. Bowden, J. A. Harrington, and O. Mitrofanov, "Silver/polystyrene-coated hollow glass waveguides for the transmission of terahertz radiation," *Opt. Lett.*, vol. 32, no. 20, pp. 2945–2947, 2007.

[16] T. Hidaka, H. Minamide, H. Ito, S. I. Maeta, and T. Akiyama, "Ferroelectric PVDF cladding THz waveguides," *J. Lightw. Technol.*, vol. 23, no. 8, pp. 2469–2473, Aug. 2005.
[17] T. Hidaka, I. Morohashi, K. Komori, and H. Nakagawa, "THz wave hollow waveguide with ferroelectric PVDF polymer as the cladding material," presented at the *2000 Conf. Lasers Electro-Opt. Eur.*, paper CWF7, 2000.
[18] K. Wang and D. M. Mittleman, "Metal wires for terahertz wave guiding," *Nature*, vol. 432, no. 7015, pp. 376–379, 2004.
[19] S. A. Maier, S. R. Andrews, L. Martin-Moreno, and F. Garcia-Vidal, "Terahertz surface plasmon-polariton propagation and focusing on periodically corrugated metal wires," *Phys. Rev. Lett.*, vol. 97, no. 17, 2006, Art. no. 176805.
[20] M. Wachter, M. Nagel, and H. Kurz, "Metallic slit waveguide for dispersion-free low-loss terahertz signal transmission," *Appl. Phys. Lett.*, vol. 90, no. 6, 2007, Art. no. 061111.
[21] R. Mendis and D. M. Mittleman, "An investigation of the lowest-order transverse-electric (TE_1) mode of the parallel-plate waveguide for THz pulse propagation," *J. Opt. Soc. Amer. B*, vol. 26, no. 9, pp. A6–A13, 2009.
[22] A. Y. Nikitin, F. Guinea, F. J. García-Vidal, and L. Martín-Moreno, "Edge and waveguide THz surface plasmon modes in graphene micro-ribbons," *Phys. Rev. B*, vol. 84, no. 16, pp. 1401–1408, 2011.
[23] H. Haroyan, Y. Avetisyan, and M. Tonouchi, "Sub-wavelength plasmonic mode confinement in semiconductor-gap-dielectric waveguide in THz range," in *Proc. Lasers Electro-Opt.*, 2011, pp. 1–2.
[24] S. Li, M. M. Jadidi, T. E. Murphy, and G. Kumar, "Terahertz surface plasmon polaritons on a semiconductor surface structured with periodic V-grooves," *Opt. Express*, vol. 21, no. 6, pp. 7041–7049, 2013.
[25] Y.-S. Lee, *Principles of Terahertz Science and Technology*, vol. 170. Berlin, Germany: Springer, 2009.
[26] L. Smith *et al.*, "THz field enhancement by antenna coupling to a tapered thick slot waveguide," *J. Lightw. Technol.*, vol. 32, no. 20, pp. 3676–3682, Oct. 2014.
[27] H. Zhan, R. Mendis, and D. M. Mittleman, "Subwavelength confinement of THz radiation in tapered plasmonic slot waveguides," in *Proc. 2010 Conf. Lasers Electro-Opt. Quantum Electron. Laser Sci. Conf.*, 2010, pp. 1–2.
[28] Y. Bian and Q. Gong, "Long-range hybrid ridge and trench plasmonic waveguides," *Appl. Phys. Lett.*, vol. 104, no. 25, Jun. 2014, Art. no. 251115.
[29] Y. Bian and Q. Gong, "Metallic-nanowire-loaded silicon-on-insulator structures: A route to low-loss plasmon waveguiding on the nanoscale," *Nanoscale*, vol. 7, no. 10, pp. 4415–4422, 2015.
[30] Y. S. Bian, Z. Zheng, X. Zhao, J. S. Zhu, and T. Zhou, "Symmetric hybrid surface plasmon polariton waveguides for 3D photonic integration," *Opt. Express*, vol. 17, no. 23, pp. 21320–21325, Nov. 2009.
[31] Y. Song, M. Yan, Q. Yang, L.-M. Tong, and M. Qiu, "Reducing crosstalk between nanowire-based hybrid plasmonic waveguides," *Opt. Commun.*, vol. 284, no. 1, pp. 480–484, Jan. 2011.
[32] G. Veronis and S. Fan, "Crosstalk between three-dimensional plasmonic slot waveguides," *Opt. Express*, vol. 16, no. 3, pp. 2129–2140, Jan. 2008.

Jing Xiao received the M.S. degree in electronic engineering and automation from Guilin University of Electronic Technology, Guilin, China and the Ph.D. degree in optical engineering from BeiHang University, Beijing, China, respectively.

He is currently a Professor in the Guilin University of Electronic Technology, where he is involved in studying the performance of micro/nano-structure optical devices and its packaging technology. His Ph.D. research was on the mirco/nano-functional structure based on the field enhancement surface plasmon plariton for use in telecommunication and solar energy applications. His research interests include heterogeneous integration of silicon and optical interconnect of board level.

Qi-Qin Wei received the B.S degree from the Guilin University of Electronic Technology, Gulin, China. He is currently working toward the M.S. degree from the School of Electronic Mechanical and Electrical Engineering, Guilin University of Electronic Technology. His research interests include heterogeneous integration of silicon for optical interconnect.

Duo-Guo Yang is a Professor at the Guilin University of Electronic Technology, Gulin, China. He is currently working on microelectronic packaging technology.

Ping Zhang receive the Ph.D. degree from Nanjing University of Science and Technology, Nanjing, China. He currently investigates the cooling of electronic systems.

Ning He is a Professor at the Guilin University of Electronic Technology, Gulin, China.

Guo-Qi Zhang is a Professor in the Delft Institute of Mircosystems and Nanoeleconics, Delft University of Technology Delft, The Netherlands.

Xian Ping Chen is a Professor in the College of Optoelectronic Engineering, Chongqing University, Chongqing, China. He is developing novel mirco/nanoscale electronic devices and systems, include novel semiconductor material and devices, mirco/nano-scale sensors, light emitting diode packaging, and reliability.